

A machine-vision sensor for prawn aquaculture

Volker Hilsenstein
CSIRO ICT Centre
1 QCAT Technology Ct
Pullenvale, QLD 4069, Australia
Volker.Hilsenstein@csiro.au

Rongxin Li
CSIRO ICT Centre
Cnr Pembrook Rd and Vimiera Rd
Marsfield, NSW 2122, Australia
Ron.Li@csiro.au

John McCulloch
CSIRO Tasmanian ICT Centre
Castray Esplanade
Hobart, TAS 7000, Australia
John.McCulloch@csiro.au

Abstract—We present a machine vision system for monitoring prawns in aquaculture ponds, developed as a tool to study feed consumption and prawn size distributions. We discuss design objectives and propose a vision system comprising two wide angle cameras. Cameras and lighting system operate in the near infrared to obtain controlled illumination even in the presence of sunlight. We discuss effects of refractive index boundaries in underwater imaging and their relevance for camera calibration. Image analysis algorithms for segmenting prawns and pellets are outlined. We use a relaxed epipolar constraint for stereo correspondence search in the presence of residual aberrations caused by refraction. Field trials were conducted in different settings and we report results obtained during these deployments.

I. INTRODUCTION

A. Background and Aim

Driven by the increase in demand for seafood and the decline of wild fisheries, marine aquaculture has become one of the fastest growing industries worldwide, with annual growth rates of close to 15% for crustaceans during the 2000-2008 period [1]. Over the last decade, some areas of aquaculture, in particular salmon and tuna farming, have benefited from the introduction of farm automation and monitoring equipment, including video-based sensors ranging from remote feeding and environmental monitoring systems (e.g. AQTV pro, AK-VAGroup akvasmart) to underwater stereo camera systems for fish sizing (e.g. AQ1 Systems AM100).

To date many of these advances for fish farming have not been implemented in prawn aquaculture. Unlike fish, prawns spend time on the bottom of ponds foraging and feeding. Husbandry techniques encourage algae blooms and other sources of turbidity in ponds. The resulting limited visibility combined with the bottom dwelling behaviour present unique challenges, preventing the video techniques commonly used in fish farming from being successful for monitoring prawn feeding and sizes.

In this paper, we present our recent work on developing a machine-vision sensor for remotely monitoring prawn behaviour, measuring prawn size and estimating prawn weight. We propose the use of image analysis to automate some of the monitoring aspects. Our aim is to develop a commercially viable system that allows the prawn farmer to save labour costs, reduce over-feeding and to allow for better management decisions by providing information about feed uptake, prawn size and weight distributions and feed conversion ratio.

B. Related work

1) *Underwater camera calibration and photogrammetry*: One of the difficulties with underwater imaging are the distortions introduced by the refraction of light at the viewport separating the camera housing from the water, in particular when the aim is to achieve metric measurements using triangulation from multiple views. This problem is a particular case of *multimedia photogrammetry*, a field with a long history starting with works from Zaar [2] and Rinner [3], see [4] for a review. Applications are also found in other fields such as oceanic engineering [5], fisheries [6], and sports biomechanics [7]. Recently, the topic has also received attention in the computer vision community [8], [9].

2) *Vision sensors in aquaculture and fisheries*: In the application domain the most similar work is in underwater photogrammetric measurements of fish, see Shortis [6] for a review. Some of the approaches described in [6] are also implemented in commercial systems, e.g. AQ1 System's AM100.

C. Overview

The remainder of this article is organised as follows: Section II describes the design constraints and the hardware of the prawn video unit. Section III describes the image analysis pipeline, including underwater calibration, image pre-processing, segmentation, feature extraction and stereo. Section IV gives an overview of results and insights obtained from various deployments of the sensor, including capturing a reference library of prawns to establish an allometric correlation between image features and prawn body weights. We present our conclusions in Section V.

II. PRAWN IMAGING SENSOR

The imaging sensor unit is shown in Figure 1. It is designed to be placed at the bottom of a pond and comprises a pair of cameras looking upward. This design is modelled on mesh feed trays, which are lowered to the bottom of the pond with feed on them and retrieved after some time. The mesh feed tray is the current tool used by farmers for assessing feed consumption by prawns. With the chosen design the video sensor acts as a replacement for the feed-tray, with the advantage that it can be monitored remotely and may also provide automated measurements of pellet consumption and prawn size.



Fig. 1. Imaging sensor unit

A. Design constraints

The hardware design was driven by partly conflicting functional and commercial requirements. Key commercial constraints were cost, weight and ease of use, whilst key functional requirements were the abilities to operate in the harsh underwater environments and to provide representative feeding and size information. In particular, the following constraints determine many aspects of the design and performance:

1) *Weight/volume restriction*: The sensor should be light enough to facilitate deployment by a single operator. This weight restriction directly corresponds to a restriction on volume as the unit needs to be negatively buoyant.

2) *Short working distance*: Two factors dictate the use of a short working distance. First, the high turbidity of the water with many particles and algae limits the range with sufficient visibility and contrast for imaging. Second, the goal of a large view window, combined with a constraint on volume can only be met with a shallow enclosure. In general, a short working distance is not desirable for metrology as it causes relatively large changes in scale for small changes in subject distance.

3) *Uncontrolled outdoor lighting*: Another commercial requirement was that the unit must be able to operate both day and night in an uncontrolled outdoor environment with associated changes in natural illumination, ranging from darkness to full sun overhead.

4) *Cost constraints*: The manufacturing and calibration costs of the unit must be low.

5) *Effect on prawn behaviour*: The sensor must not affect the behaviour of the prawns. An example for a potential disturbance from the LEDs is phototaxis, a locomotive response to light.

B. Imaging unit hardware description

1) *Housing and ballast*: The sensor unit comprises a waterproof aluminium housing with a transparent polycarbonate viewport. The inside of the unit is blackened with paint to reduce secondary reflections. For many materials, reflectance at visible and infrared wavelengths differs; care was taken to choose a paint with low reflectance for near-infrared wavelengths. Sufficient ballast is placed in the enclosure to ensure the unit has a negative buoyancy.

2) *Illumination*: The unit is equipped active illumination for the near-infrared wavelength region. Near-infrared illumination was chosen for two reasons. First, the high attenuation of light in sea water in the near infrared region offers the possibility to control lighting conditions even in the presence of sunlight. For this, we block visible wavelengths using optical filters. Second, prawns are not sensitive to near-infrared light, so the potential of the unit to affect the behaviour is reduced. The specific choice of wavelength is a trade-off determined by the spectral attenuation characteristics of the water column, the spectral sensitivity of the imaging sensor, and the availability of cheap optical filter material. Wavelengths from 810 nm to 850 nm are suitable. The LEDs were sourced from various manufacturers and are mounted at the base of the unit. The spatial arrangement and the tilt angle of the LEDs were chosen to provide uniform lighting. Due to the limited space in the enclosure and the wide angle lenses, it is not possible to position the LEDs such that direct specular reflection is avoided. Therefore, the current arrangement leads to a number of bright reflections off the polycarbonate cover. The affected regions are masked out in the subsequent image analysis.

3) *Cameras*: The unit houses a pair of USB cameras with a 1/2.5 inch format CMOS sensors (IDS uEye) and wide angle lenses (DSL-315-NIR, Sunex Inc, CA, USA) giving a horizontal view angle of 140 degrees. The hot mirror in the camera was replaced with a polycarbonate-based filter material (NIR-80N, CLAREX, Japan) that is transparent to near-infrared wavelengths but strongly attenuates visible light.

4) *Embedded computer*: We use an embedded industrial PC board for acquisition of images using the USB cameras and storage on disk. A power over Ethernet (POE) system is used as the communication and power supply to the unit. Ethernet connectivity was a requirement to facilitate real-time remote monitoring.

III. IMAGE PROCESSING

A. Camera calibration

When calibrating the camera/lens combination used in the sensor unit, two factors must be considered. First, the refractive interfaces (air/polycarbonate and polycarbonate/water) of the planar viewport need to be taken into account. Second, the DSL-315-NIR lens is a fisheye lens that exhibits strong non-rectilinear distortion typical for such optical designs.

1) *Refraction and multi-media photogrammetry*: The refractive effects for a planar viewport perpendicular to the optical axis are illustrated in Figure 2. For illustrative purposes we neglect the view window itself and only consider a single interface. A ray projected out from an image point is refracted at the interface according to Snell's law, $\frac{\sin(\theta_{\text{air}})}{\sin(\theta_{\text{water}})} = \frac{n_w}{n_a}$ where $\theta_{\text{air},\text{water}}$ and $n_{a,w}$ are the angles of incidence angles and the refractive indices for the two media, respectively. If we trace back the ray from the water side neglecting the refractive interface, it intersects the optical axis at a position d_{eff} , which we call the effective projective centre C_{eff} . The effective focal length f_{eff} is given by the distance of C_{eff} to the position

along the optical axis where the distance of the ray is equal to the distance h of the original image point from the axis. Using trigonometry we obtain $f_{\text{eff}} = \alpha(\theta_{\text{air}}, n_w, n_a) f_{\text{air}}$ and $d_{\text{eff}} = \alpha(\theta_{\text{air}}, n_w, n_a) d_{\text{air}}$ where α is a correction term that depends on the angle with the optical axis and the refractive indices of both media:

$$\alpha(\theta_{\text{air}}, n_w, n_a) = \frac{\tan \theta_{\text{air}}}{\tan \left(\sin^{-1} \left(\frac{n_a}{n_w} \sin \theta_{\text{air}} \right) \right)} \quad (1)$$

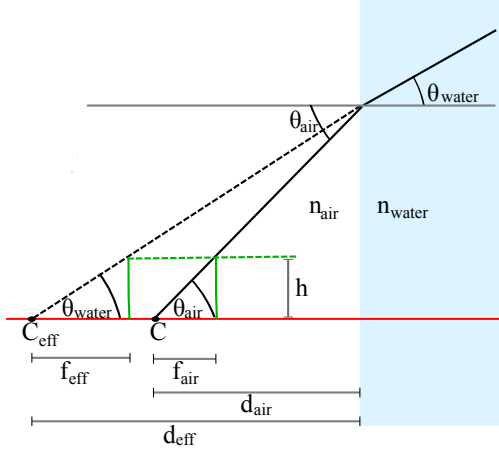


Fig. 2. Refraction at a planar interface. The projective centre C is shown on the optical axis (red). An image point that intersects the image plane (green) at a distance h from the optical axis has a view angle of θ_{air} and is refracted at the interface. If the refracted ray is backtraced without refraction, its intersection with the optical axis marks the effective projective centre C_{eff} of the refracted ray. The effective focal length f_{eff} is the distance between C_{eff} and the point where the backtraced ray is at a distance h from the optical axis. Everything is rotationally symmetric around the optical axis.

For small angles we can simplify this expression using $\tan \theta_{\text{air}} \approx \sin \theta_{\text{air}} \approx \theta_{\text{air}}$ and $n_{\text{air}} = 1$ to obtain the first-order approximation $\alpha \approx n_w$ and consequently $f_{\text{eff}} = n_w f_{\text{air}}$ and $d_{\text{eff}} = n_w d_{\text{air}}$. Thus for a narrow field of view, the refractive interface can simply be modelled by assuming a camera with a focal length multiplier of n_w moved further back from the interface by the same factor.

For medium to wide view angles, however, equation (1) has important implications. In particular the dependence of f_{eff} and of C_{eff} on the view angle θ_{air} become significant, which means that rays projected out from the centre of projection with different angles do not intersect the optical axis in a common point when back-projected. Thus, the combined optical system of camera and flat viewport is effectively a non-central camera. The net effect is similar to a pincushion distortion but with a dependence of the amount of radial distortion on distance [10].

Existing work addressing the problem of distortion for underwater camera calibration and triangulation mostly falls into two categories:

- Explicit modelling of the refractive interfaces and ray tracing, particularly for stereo and general multiple-view

camera configurations. A common approach is one of a two-stage calibration, with a first camera calibration in air to determine the intrinsics and extrinsics of multiple cameras and a second calibration in water. Optical parameters of the viewport and the media, i.e. refractive indices, position, thickness and orientation with respect to the camera are then determined by minimising reprojection errors using non-linear optimisation, see for example [5], [11]. Kotowski [12] presents a generalised bundle-adjustment method that integrates ray-tracing and refractive interfaces.

- Using standard camera calibration methods to determine camera parameters, and absorb the refractive index aberrations in the camera parameters, in particular radial distortion parameters and focal length. The advantage of this approach is that existing tools and software packages can be used. Examples are [6], [10], [13].

The preliminary results presented in this paper are based on the second approach of applying standard calibration routines and absorbing refractive effects in the camera parameters, as described in the following. We have also captured additional calibration data that will allow us to reanalyse the data with the more accurate approach of modelling the refractive index boundaries explicitly.

2) *Calibration procedure:* We use *OCamCalib* [14], a calibration toolbox for fisheye cameras which is based on imaging a planar calibration target from multiple orientations and to solve for the camera parameters and the homographies simultaneously, similar to [15]. As input for OCamCalib we use a set of images of a screen-printed acrylic chessboard target backlit by an array of LEDs. Both the sensor unit and the calibration target are submerged in water for image capture. As the refraction-induced radial distortions are distance-dependent we only use images of the calibration target within a narrow range of distances close to the sensor viewport (1 cm - 4 cm, about the height of a prawn) and small amounts of tilt. This is in contrast to recommended calibration procedures in air where a wider range of distances and orientations helps to better constrain the solution. We first calibrate both cameras independently and then determine extrinsic parameters from point correspondences between the two views of a calibration target. A pair of homographies for stereo rectification is obtained by remapping both image planes to a plane parallel to the sensor view port, see for example [16].

B. Pre-processing

1) *Remapping for rectification and distortion removal:* The images of the camera are remapped to correct for radial distortion and to apply homographies that project the image planes onto a plane that is parallel to the viewport and the line connecting the camera centres, thus yielding rectified images for stereo matching.

2) *Background subtraction:* We subtract a background image to remove reflections from LEDs and to identify regions of activity. For indoor tank deployments, an image taken without prawns on the unit is sufficient. For deployments

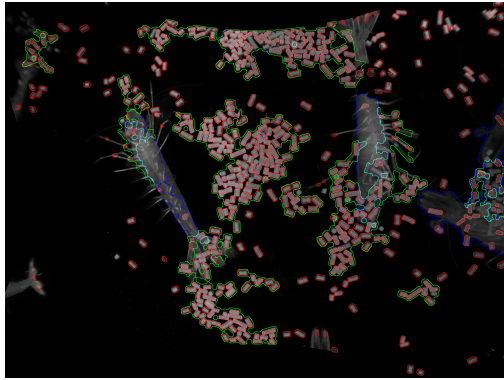


Fig. 3. Sample pellet segmentation results, detected pellets shown in red.

in outdoor ponds where there is gradual accumulation of sediment we have used a dynamic background model by simply taking the minimum grey-value for each pixel observed over the previous n frames. This simple approach is valid if sunlight is suppressed as any object moving into view can only increase the greyvalue by reflecting light from the LEDs back into the camera. If sunlight cannot be attenuated sufficiently, greyvalues can both increase and decrease and in such situations taking the median greyvalue over a n -frame history is a better approach. We maintain a binary mask image of areas with overexposed and saturated pixels resulting from specular reflections of LEDs.

C. Segmentation of pellets

For the segmentation of pellets we make use of the known pellet size and shape by setting limits on the minimum and maximum width and length of the pellet. In a first step we use a morphological opening with a circular structuring element to remove structures smaller than the minimum pellet radius. Then we use a morphological area top-hat filter [17] to detect candidate pellets, using pellet area as a filter criterion.

D. Segmentation of prawns

Prawns are segmented to obtain an estimate of their size. Given the controlled lighting and making the assumption that a large number of prawns will be recorded by the sensor unit, we employed a simple threshold-based segmentation approach combined with aggressive filtering to only retain prawns that are isolated and fully visible, i.e. not connected to other prawns, larger patches of pellets or the image boundary. The prawn segmentation consists of the following steps:

1) *Connected component analysis and filtering:* Following background subtraction (see Section III-B2), connected components are extracted from each image following a morphological opening and binarisation using an intensity threshold. We filter the connected components based on area and shape attributes to remove patches of pellets, sediment and other noise that is not removed by the background model. The image boundaries are padded with a foreground value such that any prawn connected to the boundary (and thus only partially visible) is discarded. An example image after background

subtraction and segmentation results after filtering are shown in Figure 4.

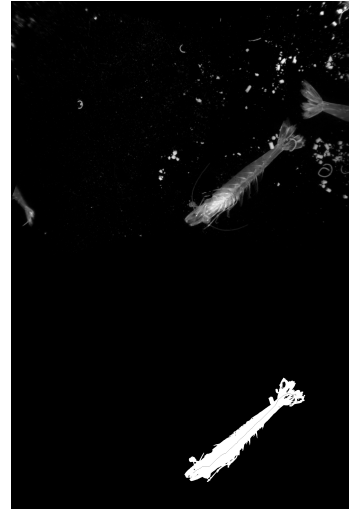


Fig. 4. Image after remapping and background subtraction (top) and segmentation results with overlaid pruned skeleton (bottom).

E. Feature Extraction

Once prawn masks have been obtained, we extract image-based features that are correlated with physical body length and weight of the prawn, see Section IV-A1. In addition to simple features such as image area we compute a skeleton-based measure as an approximation for prawn length.

1) *Skeletonisation, pruning and identification of key points:* Following the above filtering process each connected component is skeletonised using a digital topology algorithm [18] that iteratively removes points that are simple and non-terminal [19], with the order of the removal being determined by a chamfer distance transform. Short, non-bifurcation stubs are pruned to improve robustness of the next stage calculation. An example is shown in Figure 4.

Based on their connectivity, all end points and all major branching points on the skeleton are identified. The two ends of the prawn are identified by a pair of points consisting of the one end point and the one major branching point with the largest distance from one another. The distance along a straight line between the point pair is taken as the length measurement, which is subsequently used to derive image-based allometric relations, see Section IV-A1.

2) *Additional image features:* The area in pixels of a prawn's binary mask, the best fitting ellipsoid and an axis-aligned bounding box are also computed as supplementary features.

F. Stereo matching

A number of factors make it difficult to measure the physical length of a prawn accurately with a single projective image. Importantly, scale cannot be established without knowing the distance of the prawn from the sensor. The large changes of scale with subject distance due to the short working distance

exacerbate this problem. Other limiting factors include the non-rigidity of prawns and different view angles associated with different positions on the sensor.

We intend to use stereo-based triangulation to establish the distance and pose of the prawn with respect to the camera and to correct length measurements accordingly. To this end we have investigated the viability of automatically identifying feature point correspondences between individual prawns. One of the difficulties in this regard is that the epipolar constraint, which is commonly used to constrain the search space for correspondences, cannot be applied in its usual form due to refraction at the viewport. Consider a refracted ray spanned by an image point and the projective centre in one camera. When this ray is projected into the other camera, the resultant projection is not a straight line. Instead of searching along the resultant projection, we relax the epipolar constraint to allow correspondences to fall within a narrow band of pixels as opposed to a single scanline. A similar approach has been described in [13]. While this approach does not lend itself to dense matching we have found it effective when using point based matching. We implemented feature-point based matching for interest points detected using SURF [20] and nearest-neighbour matching on the descriptor vectors using the OpenCV library [21]. An example result is shown in Figure 5. We intend to use the 3D coordinates obtained for matched interest point pairs within segmented prawns to apply pose-based corrections to the length estimate obtained using the 2D skeleton. Such an approach is necessary as we cannot derive length measurements from the feature points directly, since there are no guarantees that the SURF interest points will coincide with end points of the prawn.

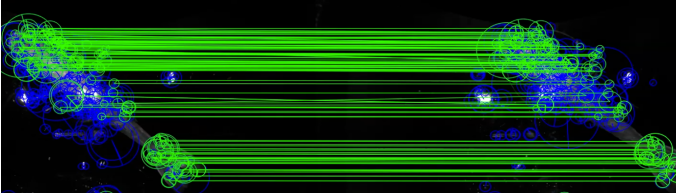


Fig. 5. Stereo matching using SURF interest points and relaxed epipolar constraint.

IV. SENSOR DEPLOYMENTS AND EXPERIMENTAL RESULTS

We have trialled the sensor unit in different environments, ranging from indoor tanks as detailed in Section IV-A and different types of outdoor ponds ranging from small research ponds of up to 20 m by 20 m in area, with concrete or lined base and sides Section IV-B to large commercial ponds up to 100 m by 100 m in area, with mud base.

A. Indoor experiments

Prior to outdoor field deployments, we conducted a number of experiments in indoor prawn tanks at the CSIRO Marine and Atmospheric research facility in Cleveland, QLD, Australia, to test the viability of the imaging sensor unit and to calibrate the imaging units in water. In general, the conditions in indoor

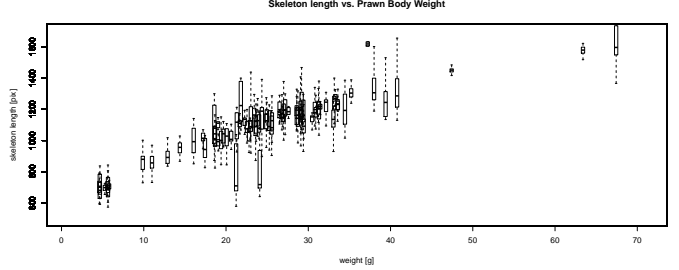


Fig. 6. Skeleton-length from image based measurements versus prawn weight. The boxplots represent the distribution of skeleton lengths derived from different images of an individual prawn.

facilities are more amenable to automated imaging as there is no uncontrolled sunlight and no sediment deposition on the sensor. The image data obtained from these experiments indicated that we could acquire images of good quality to allow for automated detection of pellets and prawns. During a month-long deployment we were able to track pellet numbers reflecting feeding times and typical pellet consumption cycles. A sample image from this deployment is shown in Figure 3.

1) *Allometric reference library*: Direct measurements of individual prawn weight in the pond are difficult to perform automatically due to the buoyancy and the need to capture the prawns. While image-based measurements do not give direct access to prawn weight either, correlations between length and weight can be used to derive weight estimates. Observed average dependencies between length and weight of an animal are captured in so-called *allometric* relationships. For black tiger prawns such relationships are reported by Primavera et al [22]. To determine similar allometric relationships between prawn-weight and image based features we captured a reference image set of 90 prawns covering a range of weights from 4.6 g to 68 g.

We captured a set of images where we placed the imaging sensor in a small tank and individually placed each prawn on the sensor for several minutes, during which we recorded a series of 50 frames. In addition, manual measurements of weight and various length features were taken. The images of each prawn were analysed as outlined in Section III-E. The resulting relationship between the image-based length feature and prawn weight is shown in Figure 6, where each box-and-whiskers represents the distribution of length measurements for different images of a single prawn. As is visible from the boxplots, the observed variation in skeleton length extracted from different images of the same prawn is relatively large. We attribute this to changes in prawn pose, as well as distance and position with respect to the camera. It is expected that the inclusion of the 3D information from stereo will yield measurements with less variation. When only the median length measurement for each prawn, indicated by the centre line in the box plot, is considered the overall shape of the allometric relationship is similar with allometric relationships reported in [22].

B. Outdoor experiments

Over the months of February to April 2011, we deployed prototype units in several outdoor ponds in south-east Queensland for periods ranging from several hours up to a week. The deployment sites included a research pond and several ponds at commercial farms. Our observations from these deployment confirm that the approach of using near infrared lighting in combination with filters attenuating visibly wavelengths is effective even in harsh outdoor conditions. Direct sunlight was sufficiently attenuated in all but one experiments (a pond that was very shallow and untypically clear). Sediment build-up on the unit was noticed as a significant problem in some, but not all of the deployments. The severity of the sediment build-up varied strongly between lined ponds (little sediment) and mud-based ponds (more sediment). We also observed variation of sediment within single ponds, with units in some locations affected more than others. A plausible explanation for this is that water currents within the pond will cause spatially varying sediment transport. Other observations that are also likely to be due to water currents include spatial variation in pellet retention on the units, and a often higher speed with which observed prawns move. The latter effect leads to a larger fraction of images affected by motion blur compared to indoor experiments.

V. DISCUSSION AND CONCLUSIONS

The presented prototype machine vision sensor for prawn aquaculture addresses many of the challenges of operating in a murky underwater environment. In particular we were able to record consistent images under challenging outdoor lighting conditions. We have demonstrated algorithms for pellet and prawn segmentation. The pellet segmentation algorithm was successfully used to track feeding cycles and pellet consumption over several weeks during deployment in an indoor tank. In large commercial prawn ponds, we observed that pellet deposition on the sensor and pellet retention vary from site to site, presumably due to variations in current. It is likely that observations obtained using the feed tray (as currently used by farmers) are similarly affected by these factors.

We created a reference image library of prawns covering a range of weights for the purpose of generating an allometric relationship between automated image-based length measurements and prawn weight. The observed variation between individual measurements are too large to constrain the weight of a prawn sufficiently based on a single measurement. We have outlined a path using stereo-based 3D measurements that is likely to reduce this variation which is partly caused by changes in scale and pose. Even with current 2D-based image features, the use of a large number of individual prawn measurements may still yield meaningful estimates of prawn weight distributions in a pond, but the required statistical analysis is outside of the scope of this paper.

ACKNOWLEDGMENT

This work is a result from a collaboration between AQ1 Systems Hobart and CSIRO and has been funded by an

Australian Growth Partnership and the CSIRO Food Futures Flagship. The authors would like to thank P. Jansen and T. Pitmann of AQ1 Systems; S. Hrabar, J. Whitham, B. Wood, L. Overs, D. Haddon, P. Borges, P. Alexander at CSIRO QCAT; A. Wood and S. Tabrett of CSIRO Marine and Atmospheric Research; D. Farrant of CSIRO Lindfield; R. Lagerstrom and L. Bischof of CSIRO MIS for their help with various aspects of the project.

REFERENCES

- [1] UN Food and Aquaculture Organization, "The state of world fisheries and aquaculture 2010," 2010. [Online]. Available: <http://www.fao.org/docrep/013/i1820e/i1820e.pdf>
- [2] K. Zaar, "Zweimediengesamtmetrie," *Öster. Zeitschrift f. Vermessungswesen*, no. Sonderheft 4, 1948.
- [3] K. Rinner, "Problems of two-medium photogrammetry," *Photogrammetric Engineering*, no. Sonderheft 4, 1969.
- [4] H. Maas, "New developments in multimedia photogrammetry," *Optical 3-D Measurement Techniques III*, 1995.
- [5] R. Li, H. Li, W. Zou, R. Smith, and T. Curran, "Quantitative photogrammetric analysis of digital underwater video imagery," *Oceanic Engineering, IEEE Journal of*, vol. 22, no. 2, pp. 364 – 375, 1997.
- [6] M. Shortis, E. Harvey, and J. Seager, "A review of the status and trends in underwater videometric measurement," in *Proceedings SPIE Electronic Imaging, Conference 6491, Videometrics IX*, San Jose, CA, USA, Jan 2007.
- [7] Y.-H. Kwon and R.-J. Sung, "A comparative biomechanical evaluation of the start techniques of selected korean national swimmers," *Korean Journal of Sport Science*, vol. 7, 22-34 1995.
- [8] Treibitz, "Flat refractive geometry," *Computer Vision and Pattern Recognition, 2008. CVPR 2008. IEEE Conference on*, pp. 1 – 8, 2008.
- [9] V. Chari and P. Sturm, "Multi-view geometry of the refractive plane," *Proceedings of the 20th British Machine Vision Conference*, 2009.
- [10] Y.-H. Kwon, "Object plane deformation due to refraction in two-dimensional underwater motion analysis," *Journal of Applied Biomechanics*, vol. 15, pp. 396–403, 1999.
- [11] X. Ke, M. Sutton, S. Lessner, and M. Yost, "Robust stereo vision and calibration methodology for accurate three-dimensional digital image correlation measurements on submerged objects," *Journal of Strain Analysis*, vol. 43, pp. 689–704, 2008.
- [12] R. Kotowski, "Phototriangulation in multimedia photogrammetry," *ISPRS Archives (Papers of the XVIth Congress, Kyoto, 1988, Technical Comission V)*, vol. XXVII Part B5, 1988.
- [13] M. Dunbabin, P. Corke, and G. Buskey, "Low-cost vision-based AUV guidance system for reef navigation," *IEEE International Conference on Robotics and Automation*, Jan 2004.
- [14] D. Scaramuzza and R. Siegwart, "A new method and toolbox for easily calibrating omnidirectional cameras," in *Proc. of The International Conference on Computer Vision Systems (ICVS), Workshop on Camera Calibration Methods for Computer Vision Systems*, 2007.
- [15] Z. Zhang, "A flexible new technique for camera calibration," *IEEE Trans. Pattern Anal. Mach. Intell.*, vol. 22, no. 11, pp. 1330–1334, 2000.
- [16] R. I. Hartley and A. Zisserman, *Multiple View Geometry in Computer Vision*, 2nd ed. Cambridge University Press, ISBN: 0521540518, 2004.
- [17] L. Vincent, "Morphological area openings and closings for grey-scale images," in *NATO Shape in Picture Workshop*. Driebergen, Netherlands: Springer, September 1992, pp. 197–208.
- [18] J. Lamy, "Digital topology," *Insight Journal*, August 2006.
- [19] G. Bertrand, "Simple points, topological numbers and geodesic neighborhoods in cubic grids," *Pattern Recognition Letters*, pp. 1003–1011, 1994.
- [20] H. Bay, T. Tuytelaars, and L. V. Gool, "Surf: Speeded up robust features," in *In ECCV*, 2006, pp. 404–417.
- [21] G. Bradski, "The OpenCV Library," *Dr. Dobb's Journal of Software Tools*, 2000.
- [22] J. Primavera, F. Parado-Estepa, and J. Lebata, "Morphometric relationship of length and weight of giant tiger prawn penaeus monodon according to life stage, sex and source," *Aquaculture*, 1998.